The Horizontal Branch Population of NGC 1851 as Revealed by the Ultraviolet Imaging Telescope (UVIT)

Annapurni Subramaniam[1], Snehalata Sahu[1], Joseph E. Postma[2], Patrick Côté[3], J. B. Hutchings[3], N. Darukhanawalla[3], Chul Chung[4], S. N. Tandon[1,5], N. Kameswara Rao[1], K. George[1], S. K. Ghosh[6,7], V. Girish[8], R. Mohan[1], J. Murthy[1], A. K. Pati[1], K. Sankarasubramanian[1,8,9], C. S. Stalin[1], and S. Choudhury[10]

[1] Indian Institute of Astrophysics, Koramangala II Block, Bangalore-560034, India; purni@iiap.res.in
[2] University of Calgary, 2500 University Drive NW, Calgary, Alberta Canada
[3] National Research Council of Canada, Herzberg Astronomy and Astrophysics Program, 5071 West Saanich Road, Victoria, BC, V9E 2E7, Canada
[4] Center for Galaxy Evolution Research, Yonsei University, Seoul 03722, Korea
[5] Inter-University Centre for Astronomy and Astrophysics, Pune, India
[6] National Centre for Radio Astrophysics, Pune, India
[7] Tata Institute of Fundamental Research, Mumbai, India
[8] ISRO Satellite Centre, HAL Airport Road, Bangalore 560017, India
[9] Center of Excellence in Space Sciences India, Indian Institute of Science Education and Research (IISER), Kolkata, Mohanpur 741246, West Bengal, India
[10] Yonsei University Observatory, 120-749, Seoul, Korea

Abstract

We present the UV photometry of the globular cluster NGC 1851 using images acquired with the Ultraviolet Imaging Telescope (UVIT) onboard the *ASTROSAT* satellite. Point-spread function fitting photometric data derived from images in two far-UV (FUV) filters and one near-UV (NUV) filter are used to construct color–magnitude diagrams (CMDs), in combination with *HST* and ground-based optical photometry. In the FUV, we detect only the bluest part of the cluster horizontal branch (HB); in the NUV, we detect the full extent of the HB, including the red HB, blue HB, and a small number of RR Lyrae stars. UV variability was detected in 18 RR Lyrae stars, and three new variables were also detected in the central region. The UV/optical CMDs are then compared with isochrones of different age and metallicity (generated using Padova and BaSTI models) and synthetic HB (using helium-enhanced Y^2 models). We are able to identify two populations among the HB stars, which are found to have either an age range of 10–12 Gyr, or a range in Y_{ini} of 0.23–0.28, for a metallicity of [Fe/H] = −1.2 to −1.3. These estimations from the UV CMDs are consistent with those from optical studies. The almost-complete sample of the HB stars tends to show a marginal difference in spatial/azimuthal distribution among the blue and red HB stars. Thus, this study showcases the capability of UVIT, with its excellent resolution and large field of view, to study the hot stellar population in Galactic globular clusters.

Key words: globular clusters: individual (NGC 1851) – Hertzsprung–Russell and C–M diagrams – stars: horizontal-branch

Supporting material: data behind figure

1. Introduction

Globular clusters (GCs) have long been considered simple stellar populations, composed of stars having nearly identical ages and chemical compositions. However, a succession of studies carried out during the past decade have established that many clusters deviate from these assumptions (see, e.g., Piotto 2009; Piotto et al. 2012). NGC 1851 is one such object. Several photometric and spectroscopic studies have concluded that this cluster contains multiple stellar populations (e.g., Milone et al. 2008; Carretta et al. 2011; Gratton et al. 2012). The cluster is also remarkable in that it appears to be surrounded by a diffuse stellar halo extending to radii of ∼250 pc (Olszewski et al. 2009).

An early study of the cluster by Walker (1992) found its core, although unresolved, to have an unusually blue color. At the same time, the horizontal branch (HB) was found to be clearly bimodal, with both a red clump and an extended blue tail. Subsequent *HST*/ACS photometry of the cluster from (Milone et al. 2008) revealed the existence of two distinct sub-giant branches (SGBs) as well. These authors found the bright SGB component to outnumber the fainter component by ∼10%, and

that the percentages of red and blue HB stars are 63% (RHB) and 37% (BHB), respectively. These multiple SGB populations were interpreted as evidence for two populations having either an age difference of about 1–2 Gyr or a significant difference in their C + N + O content (Cassisi et al. 2008; Piotto et al. 2012). Salaris et al. (2008), on the basis of detailed synthetic modeling of HB stars, concluded that these two populations are distributed in different regions of the HB. The evolved stars, belonging to the bright SGB component, are confined to the red portion of HB, whereas the the faint SGB population have HB stars distributed from the blue to the red, even populating the RR Lyrae instability strip. Salaris et al. (2008) also argued that large variations in the initial He abundance between the two sub-populations could be ruled out.

Gratton et al. (2012) studied the chemical composition and Na-O anti-correlation of HB stars from moderately high-resolution spectra for 91 stars on the bimodal HB and 13 stars on the red giant branch (RGB). This spectroscopic study found that the RHB stars divide into two groups, with the vast majority of stars being Na-poor and O-rich. About 10%–15% of the stars are Na-rich and moderately O-poor, with most, but not all, being Ba-rich. The two groups were found to occupy
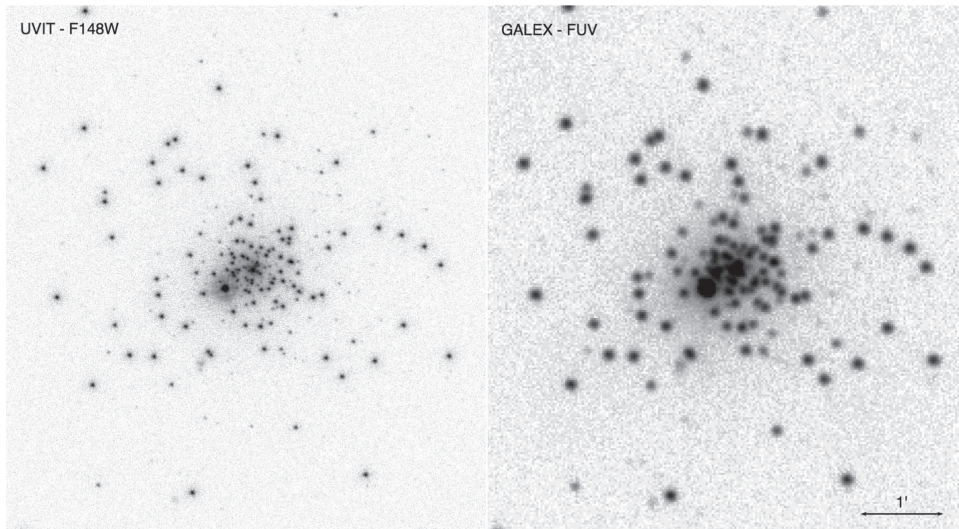
Figure 1. Comparison of FUV images for NGC 1851 taken with UVIT and *GALEX* (left and right panels, respectively). The UVIT image was constructed from a total integration time of 6982.13 s in the F148W filter. North is up and east is to the left. Only a subset of the full image is shown in each case.

distinct regions of the color–magnitude diagram (CMD), where the Na-rich stars are redder and slightly brighter than the Na-poor ones. They found the BHB stars to be enriched in N, but not exceptionally so, and the total CNO abundance unlikely to be anomalous. The He abundance of the BHB was found to be consistent with both the cosmological value and a small He enhancement. This confirmed the lack of evidence for very large He enhancements within NGC 1851. Their study identified an age spread of ∼1.5 Gyr as the only viable explanation for the split of the SGB. It also suggested that most of the BHB stars are older than their RHB counterparts, based on their computed synthetic HB and adopting the bright and faint SGB fractions of Milone et al. (2008).

This conclusion is in agreement with the findings of Carretta et al. (2011), who first suggested that the cluster might be the product of a merger between two GCs having an age difference of ∼1 Gyr. Han et al. (2009) modeled the HB stars and suggested that the presence of bimodal HB distribution in NGC 1851 can be naturally reproduced if the metal-rich second-generation stars are also enhanced in helium. Joo & Lee (2013) later argued that the two populations were similar in age and metallicity, but differed in He content, after comparing their (Yonsei-Yale) models with the observed CMD. Kunder et al. (2013) modeled the HB stars using He-enhanced models, and noted synthetic BHB stars, along with the RR Lyrae stars, having an increasing He content and ages ∼1.5 Gyr older than their RHB counterparts. They also argued that the cluster may be a merger remnant. Using deep *HST* imaging, Piotto et al. (2015) presented NUV-optical CMDs for a number of Galactic GCs. The CMD of NGC 1851, which is shown in their Figure 5, reveals a broad and complex HB. Yong & Grundahl (2008) also suggested that two stellar populations might exist in NGC 1851, and noted that this cluster has experienced a complicated formation history that bears some similarities to Omega Centauri. In summary, there is a general agreement that the HB population in this cluster shows an age difference, as well as small differences in [Fe/H], CNO, and He enhancement. Among the above parameters, particularly, the differences in age and He content are expected to produce similar effects in the HB morphology. Hence, it has not been possible to have a unique interpretation of HB morphology and population difference. It is also expected that the UV studies will help in alleviating this degeneracy.

The distribution of HB stars in the UV CMD can be used to better understand the formation and evolution of these stars (see, e.g., Piotto et al. 2015 and references therein). A pioneering UV study of 44 GCs using the *GALEX* images was presented by Schiavon et al. (2012), who characterized the principal features of the UV CMDs, established the locus of post-main He-burning stars in the UV CMD, and presented a catalog of candidate asymptotic giant branch (AGB), and post-AGB stars in their sample clusters. In their Figure 11, Schiavon et al. (2012) presented an FUV versus (FUV–NUV) CMD for NGC 1851 that contained a few dozen HB stars and a handful of candidate hot stars. However, due to crowding issues, this study was restricted to the region beyond the central 50″ and did not include a detailed comparison to stellar evolutionary models. In this study, we present the results of a pilot study that showcases the capability of Ultraviolet Imaging Telescope (UVIT) to study Galactic GCs by presenting the UV images, photometry that can probe the inner regions of the cluster, and the UV CMDs of NGC 1851.

The paper is arranged as follows. In Section 2, we describe the acquisition, reduction, and analysis of the UVIT images on which our study is based, including a comparison to earlier *GALEX* observations. In Section 3, we discuss the UV and optical CMDs of NGC 1851 based on our UVIT imaging, as well as *HST* and ground-based optical photometry. In Section 4, we characterize the HB populations in the cluster by comparing our UV/optical CMDs to those generated with two widely used stellar evolutionary models. In Section 4.1, we investigate the possibility of He enrichment among the BHB stars using He-enhanced models and FUV CMD. In Section 5, we explore the spatial distribution of the distinct HB populations, and in Section 6, we present the first UV light curves for RR Lyrae stars in this cluster. We conclude in Section 8.

2. UVIT Data

The images used in this study were acquired with the UVIT instrument aboard the *ASTROSAT* satellite. UVIT consists of
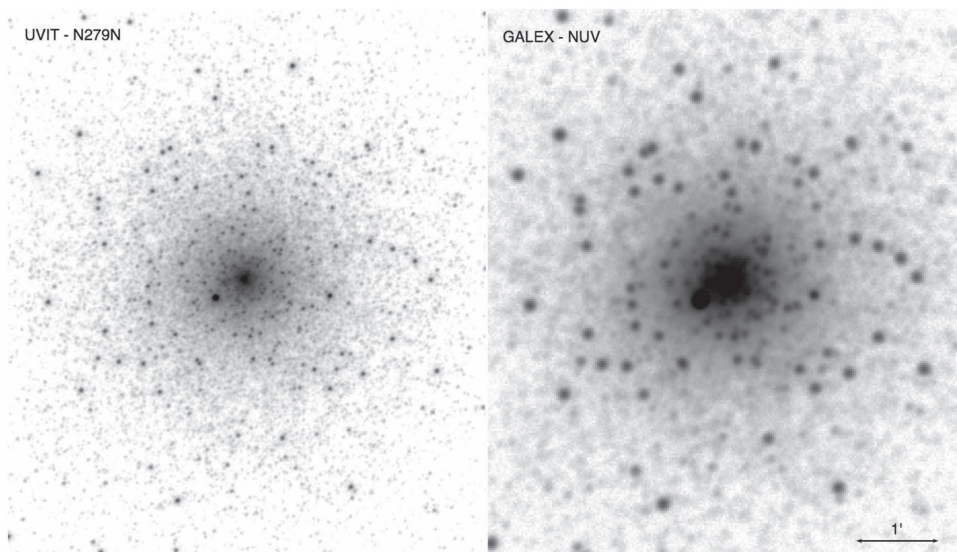
Figure 2. Comparison of NUV images for NGC 1851, taken with UVIT and *GALEX* (left and right panels, respectively). The UVIT image was constructed from a total integration time of 12234.35 s in the F279N filter. North is up and east is to the left. Only a subset of the full image is shown in each case.
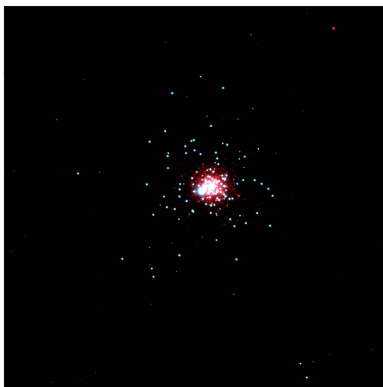
Figure 3. This color image is made from images obtained using two filters in the FUV and one filter in the NUV.

twin 38 cm telescopes—one for the FUV region (130–180 nm) and the other for the NUV (200–300 nm) and visible (VIS) regions (320–550 nm). These wavelength ranges are divided using a dichroic mirror for beam-splitting. UVIT is primarily an imaging instrument, simultaneously generating images in the FUV, NUV, and VIS channels over a circular field of diameter 28′. Each channel can be further divided using a selectable set of filters. Full details on the telescope and instruments, including initial calibration results, can be found in Tandon et al. (2017) and Subramaniam et al. (2016). The primary photometric calibration for all FUV and NUV filters were performed using observations of HZ4, a white dwarf spectro-photometric standard star (Tandon et al. 2017). The sensitivity variations across the field are calibrated to produce reliably flattened images that are accurate to within 3%, in the case of the FUV filters. The photometric accuracy is thus within 3% for FUV and within 10% in the inner regions for the NUV, due to flat-fielding errors. Based on repeated standard star observations, photometry for individual stars is accurate up to a few percent.

NGC 1851 was observed as part of UVIT's Performance Verification (PV) phase during 2016 March 19–21. The observations were part of the multi-wavelength demonstration that focused on NGC 1851 and its hot or exotic stellar content.
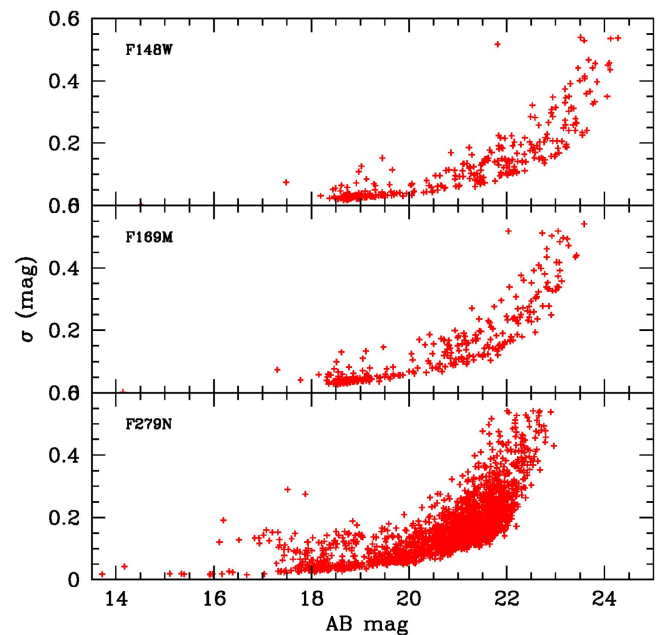
Figure 4. Photometric errors as a function of magnitude for our UVIT observations of NGC 1851. From top to bottom, the panels show results for the F148W, F169M, and N279N bandpasses, respectively.

In this study, we analyze only data from the UVIT instrument. In all, three filters were used in the program: F148W and F169M (for the FUV channel) and N279N (for the NUV). Images were corrected for geometric distortion, flat-field illumination, and spacecraft drift using our customized software package CCDLAB (Postma & Leahy 2017). In Figure 1, we compare the final FUV image from UVIT to that obtained with *GALEX*; the equivalent comparison for the NUV is shown in Figure 2. Isolated stellar sources in the UVIT images have FWHM $\sim 1{.}''5$ and $\sim 1{.}''2$ in the FUV and NUV channels, respectively. In terms of angular resolution, the UVIT images are thus far superior to those from *GALEX* ($4{.}''5$–$5{.}''5$). In the FUV, we are able to resolve stars well into the core of the cluster (although the NUV image still suffers from crowding in
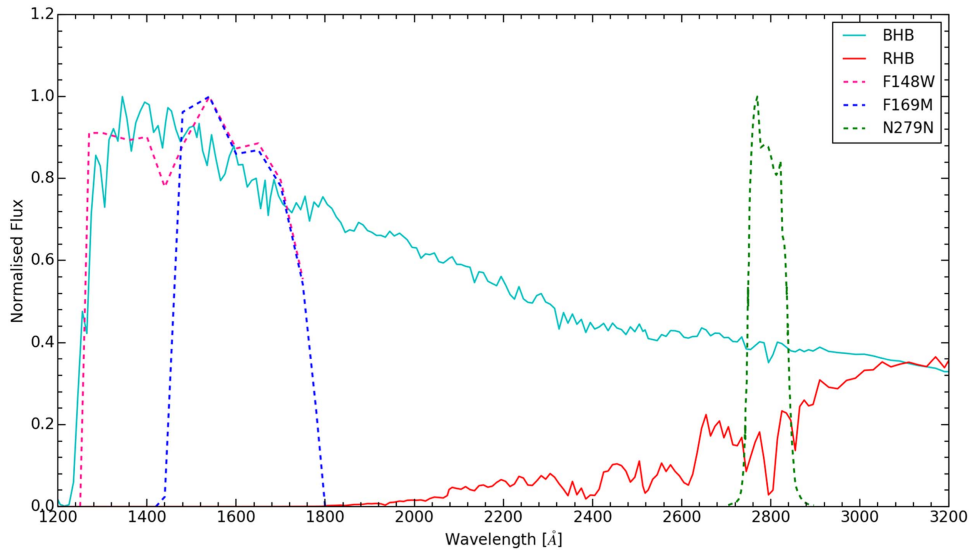
Figure 5. We have shown effective areas of the UVIT filters used in this study on a typical RHB and BHB spectra. The parameters of the BHB spectrum are $T_{\rm eff} = 10{,}790$ K, $L/L_{\odot} = 1.776$, $\mathrm{Log}(g) = 3.513$, [Fe/H] $= -1.2$, Age $= 12$ Gyr and $Y_{\rm ini} = 0.28$ and those for the RHB spectrum are $T_{\rm eff} = 5610$ K, $L/L_{\odot} = 2.713$, $\mathrm{Log}(g) = 2.492$, [Fe/H] $= -1.3$, Age $= 12$ Gyr, and $Y_{\rm ini} = 0.23$.

Table 1
Details of Photometry

Filter	$\lambda_{\rm mean}$ (Å)	Δ_{λ} (Å)	$T_{\rm exp}$ (s)	$m_{\rm zp}$ (mag)	Aperture Correction (mag)	N_{*}	UC
F148W	1481	500	6982.13	18.00	0.15	330	3.09E-15
F169M	1608	290	5274.15	17.45	0.15	306	4.39E-15
N279N	2792	90	12234.35	16.46	0.35	2298	3.50E-15

Note. The first column lists the filters used in this study. The second and third columns list the mean wavelength and the passband of the filters. The fourth column lists the exposure time, followed by the zero-point magnitude, aperture correction (mag), number of detected stars, and the unit conversion factor (to get flux in $\mathrm{erg\ cm^{-2}\ s^{-1}\ Å^{-1}}$) for the filters.

the central regions). The combined FUV+NUV false-color image of NGC 1851 is presented in Figure 3. This combined image demonstrates the capability to produce excellent resolution in both the UV channels, including satisfactory correction to satellite drift, distortion, and alignment. Finally, because the UVIT data were collected over several orbits, we are able to detect a number of variable stars in the field. In Section 6, we discuss these variables and characterize their flux variations in the UV region.

Aperture photometry was performed on the images to estimate the counts after correcting for the background. The point-spread functions (PSFs) for isolated stars were constructed and applied to all the detected stars, in order to perform PSF photometry. A curve-of-growth analysis was carried out to estimate aperture corrections in each filter, which were then applied to the PSF magnitudes. These magnitudes were calculated after applying saturation corrections. The above procedures were performed separately by two teams and consistency checks were also performed. The details of observations, photometry, and calibrations are provided in Table 1. The data presented in this study will be made available electronically. In Figure 4, we show our photometric errors as a function of PSF magnitude. Although we detect stars as faint as 23 magnitude in all filters, we have limited the comparison to the models to 22 mag in FUV and 20.5 in NUV filters. This effectively puts an upper limit of 0.2 mag on our photometric
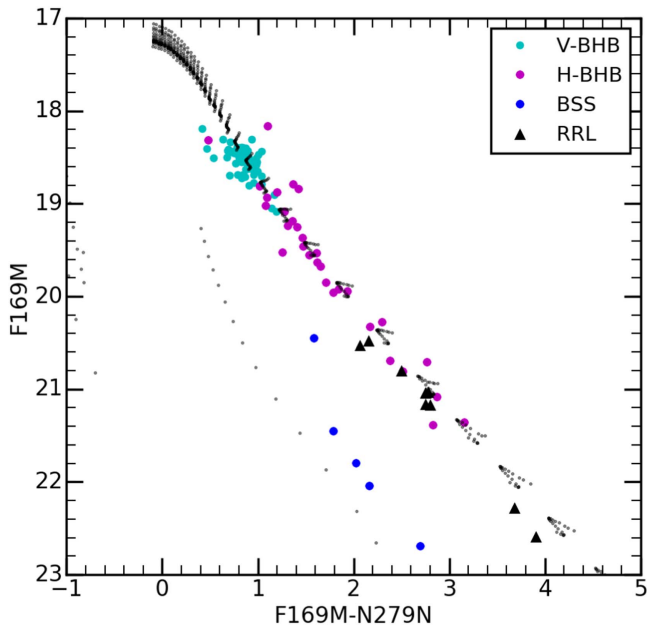
errors. Of course, as Figure 4 shows, brighter stars will have photometric errors that are considerably smaller than this.

3. The UV and Optical Color Magnitude Diagrams

The UVIT images, with their excellent resolution, allow us to resolve most stars in the central regions of the cluster (in the case of FUV images). The NUV images, on the other hand, do still exhibit crowding in the central regions. The FUV filters (F148W and F169M) are broad- and medium-band filters, whereas the NUV filter (N279N) is a narrow-band filter that is centered on the Mg II line (2800 Å). In order to show spectral coverage of the UVIT filters, we have plotted the effective filter areas on two typical BHB and RHB spectra in Figure 5. The parameters corresponding to the plotted spectra are mentioned in the figure caption. To identify and classify the stars detected with UVIT into various evolutionary phases, we used the HST/ ACS survey data for Galactic GCs (Sarajedini et al. 2007) to cross-match our stars inside a region of diameter ~3.′36. We have converted the V magnitude to the AB magnitude system, in order to make it similar to the UVIT magnitude system. These stars were found to primarily belong to the HB of the cluster. The cross-matched stars are shown in the CMD (Figures 6 and 7). The identified stars are separated into the horizontal part of the BHB (H-BHB), vertical part of the BHB (V-BHB), red part of the HB (RHB), and post-AGB stars,
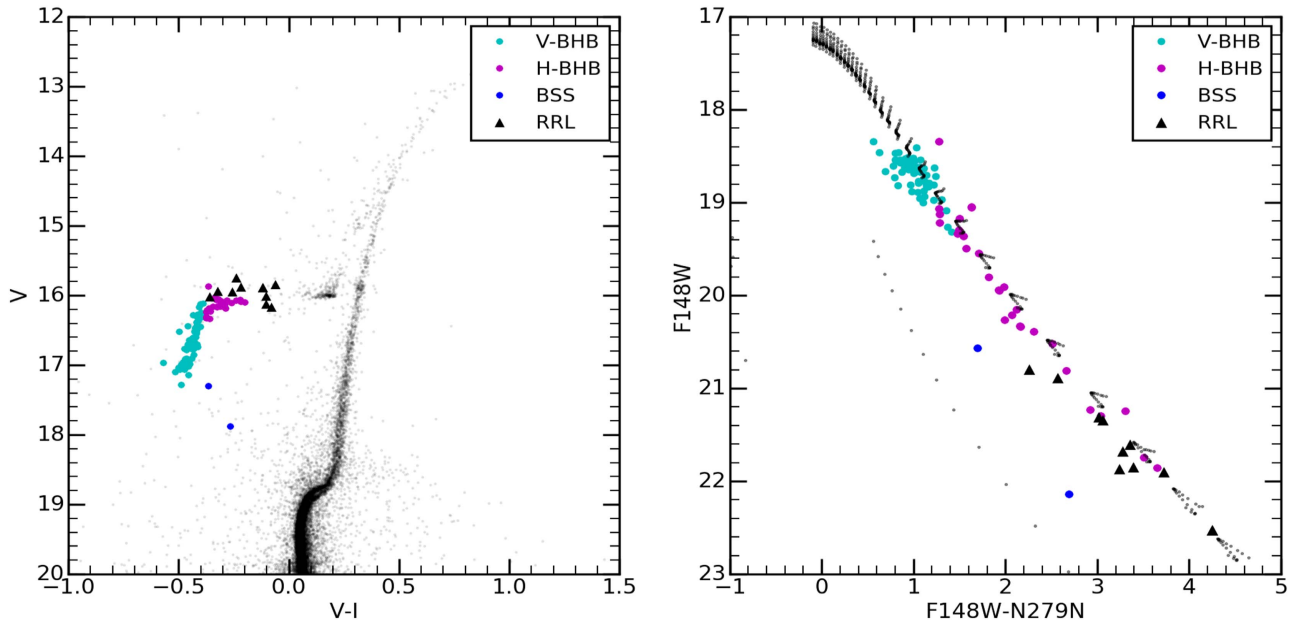
Figure 6. CMD for NGC 1851, based on F148W and N279N photometry from UVIT (right panel). For comparison, we overlay a Padova model isochrone with 10 Gyr and [Fe/H] = −1.2 dex generated using the FSPS models in the UV CMD, which are shown as black dots. The panel on the left shows the optical CMD based on *HST*/ACS photometry. Stars detected by UVIT have been separated into five components: vertical-blue horizontal branch (V-BHB), horizontal-blue horizontal branch (H-BHB), red horizontal branch (RHB) (not shown in this CMD), blue stragglers stars (BSS), and RR Lyrae stars (RRL).

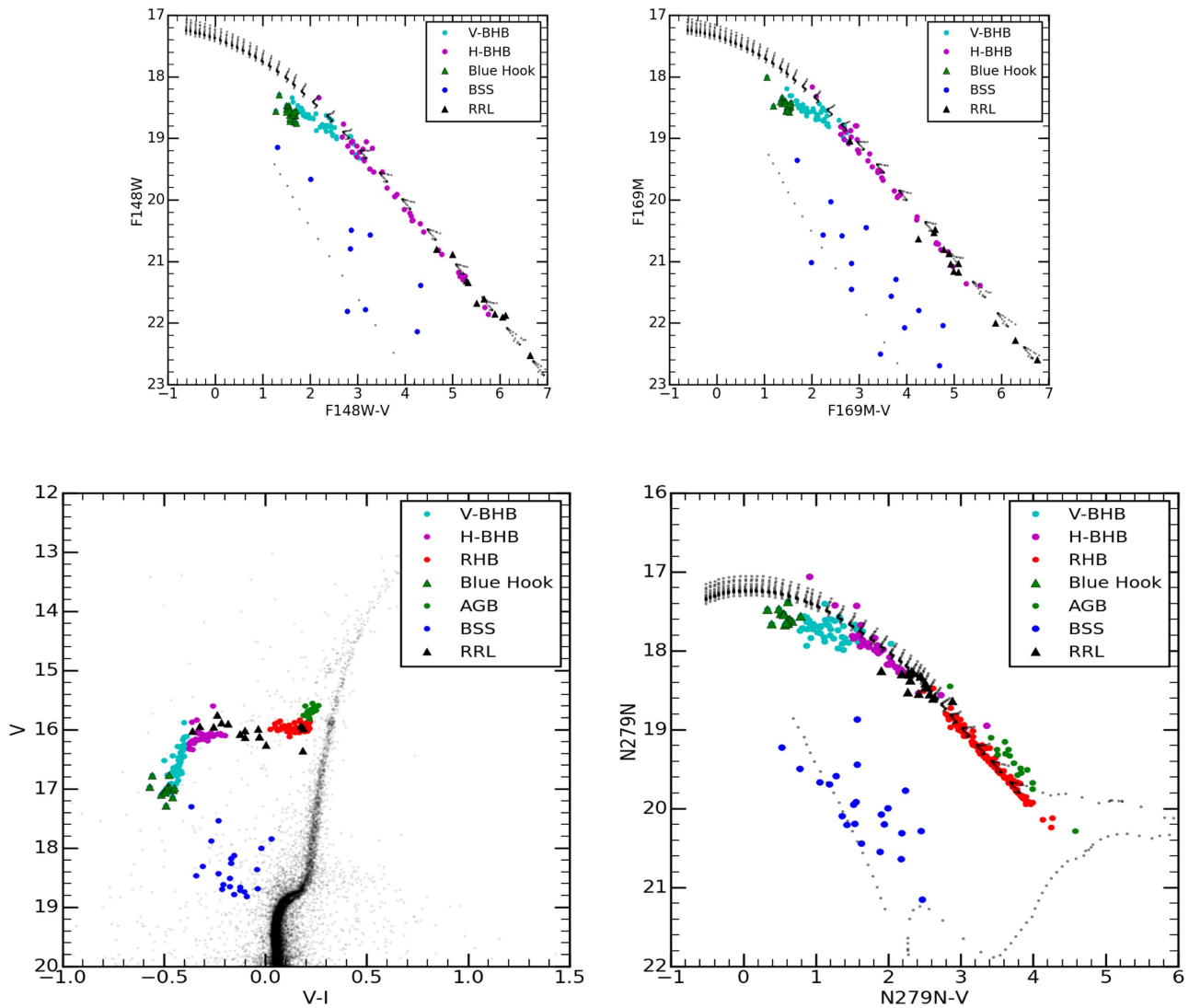
Figure 7. CMD for NGC 1851 based on F169M and N279N photometry from UVIT. For comparison, we overlay a Padova model isochrone with 10 Gyr and [Fe/H] = −1.2 dex, generated using the FSPS models in the UV CMD, which are shown as black dots. The various symbols show stars belonging to different evolutionary sequences in the CMD, as described in Figure 6.

The isochrones are generated using the Flexible Stellar Population Synthesis (FSPS) models of Conroy et al. (2009). These models include isochrone tables for the Bag of Stellar Tracks and Isochrones (BaSTI, Pietrinferni et al. 2004 and Padova isochrone sets (Marigo & Girardi 2007; Marigo et al. 2008). We used both models and filter effective area curves for the UVIT filters (Tandon et al. 2017, after incorporating the in-orbit calibrations) to generate magnitudes in our UVIT filters. The isochrones shown in Figures 6 and 7 refer to the Padova models, for a metallicity of [Fe/H] = −1.2 dex (Kunder et al. 2013), a distance modulus of 15.52 mag and an assumed age of 10 Gyr (Cassisi et al. 2008). We point out that the HB stars no longer define a horizontal sequence in the UV CMD; note that even the H-BHB gets stretched in magnitude when compared to the V-BHB.

In the right panel of Figure 6, we show all stars detected in the FUV (188 stars), from the F148W versus (F148W −N279N) CMD. In the left panel, we show the same stars in the optical CMD based on *HST* photometry. We are able to detect V-BHB and H-BHB stars, as well as five RR Lyrae stars, in the central region of the cluster, but are unable to detect RHB stars in the FUV. Hence, these stars are not present in the observed CMD. The H-BHB stars are found to closely match the isochrone, with the V-BHB stars located at the brighter end of the sequence. The V-BHB stars tend to show relatively more scatter when compared to the H-BHB stars. We also note the presence of a few H-BHB stars, as bright as the V-BHB stars. In summary, we do not see significant differences between the V-BHB and H-BHB populations, except for a large scatter in the distribution of the V-BHB stars. The RR Lyrae stars are suggestive of belonging to this population. We detected two blue stragglers, which are also shown in the figure. In Figure 7, we show the F169M versus (F169M−N279N) CMD. The corresponding optical CMD, based on *HST* photometry, is similar to that shown in the left panel of Figure 6. The principal features of the CMD are similar to those in Figure 6, suggesting

according to their location in the optical *HST*-ACS CMD. On the AB magnitude scale, V-BHB stars are those with (V − I) < −0.38, which is the starting point of this nearly vertical sequence. For comparison, BHB stars are those that have −0.38 ⩽ (V − I) < −0.17, while RHB stars have 0.02 < (V − I) < 0.22. The RR Lyrae stars detected in this study are also shown in these figures.

Figure 8. UV CMDs for NGC 1851 after cross-matching *HST*/ACS data to UVIT data in the F148W, F169M, and N279N filters. FUV CMDs are shown in the upper panels. NUV and the corresponding optical CMDs are shown in the lower panels. For comparison, we over-plot a Padova model isochrone with 10 Gyr and [Fe/H] = −1.2 dex, generated using the FSPS models in the UV CMDs, which are shown as black dots. The various symbols show stars that belong to different evolutionary sequences in the CMD, as described in Figure 6. The data used to create this figure are available.

that the V-BHB and H-BHB populations appear to be similar. We also detected five blue stragglers, which are shown as blue dots. In both the CMDs, the H-BHB is stretched to a large range of magnitude, while the V-BHB stars scatter over a smaller range.

In Figure 8, we combine the UVIT and *HST* photometry to plot UV-optical CMDs. We have shown the F148W versus (F148W−*V*) (top left panel), F169M versus (F169M−*V*) (top right panel), and N279N versus (N279N−*V*) (bottom right panel), along with the cross-matched stars in the optical CMD using the *HST* data (bottom left panel). In the UV-optical CMDs in the top panels, we detect the V-BHB, H-BHB, and some RR Lyrae stars. In the case of the bottom panel, we detect the full HB along with the RR Lyrae stars. The *HST* CMD shows all the detected stars in the NUV, whereas only a subset is detected in the FUV. The isochrones with the same age and metallicity (as in Figures 6 and 7) are shown here, for the corresponding filters. We also detect some blue straggler stars. It can be seen that, in all the three UV-optical CMDs, the

V-BHB stars deviate from the H-BHB stars. A few of the H-BHB stars are found to continue the H-BHB slope and end up brighter than the V-BHB stars. The blue hook feature can be clearly identified at the bright end of the HB in the FUV CMDs (upper panels), suggesting the presence of blue hook stars at the end of the V-BHB sequence. The H-BHB stars are found to be in a sequence, which could be an extension of the RHB stars, but we do detect some variation (bottom panel), suggesting that the H-BHB branches off with a shallower slope. As expected, the RR Lyrae stars are located between the H-BHB and RHB stars. A careful inspection reveals that the V-BHB stars can be seen to branch off from the sequence of H-BHB stars, with a bit of mixing of stars near the point of deviation. We also see that some RHB stars and H-BHB stars are mixed together, even though these groups are well-separated in the optical CMD. The RHB stars are found to have a very tight sequence with very little scatter, in comparison to the V-BHB and B-BHB stars. We find the AGB stars to be brighter than the RHB and separated from it (bottom panel).
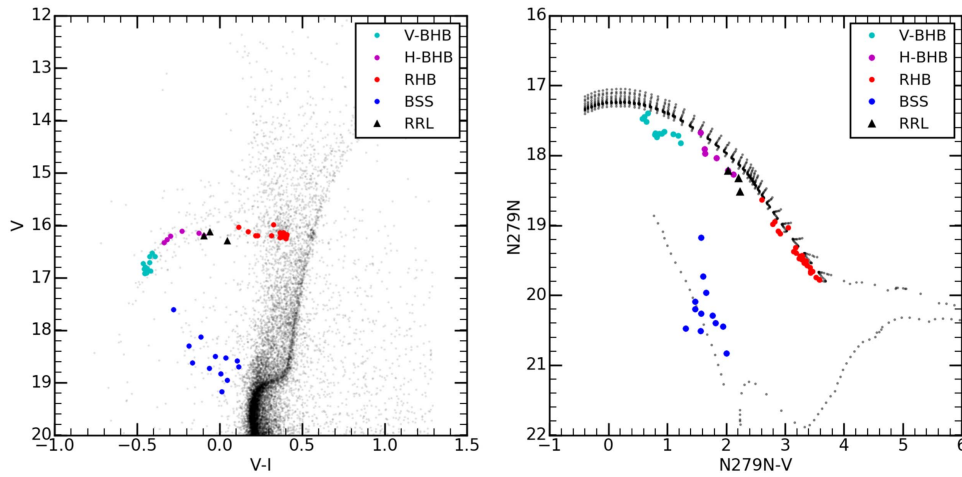
Figure 9. UV-optical CMDs obtained by cross-matching ground-based data with UVIT data in the N279N filter. For comparison, we overplot a Padova model isochrone with 10 Gyr and [Fe/H] = −1.2 dex generated using the FSPS models in the UV CMD, which are shown as black dots. The various symbols show stars belonging to different evolutionary sequences in the CMD, as described in Figure 6.

In all panels, the V-BHB stars are found to be fainter than the isochrone, whereas the B-BHB stars are almost aligned with the isochrone. This may point to some differences between these two types of stars. The RHB stars are found to extend below the magnitude limit of the HB, as delineated by the isochrone (bottom panel). This could suggest that the RHB is either metal-rich or younger than the over-plotted isochrone. We find that there could be differences among the V-BHB, H-BHB, and the RHB stars, with the V-BHB and RHB stars possibly belonging to two different populations. The differences could be due to a difference in age, metallicity, CNO abundance or mass loss, which have been mentioned as possible mechanisms by previous studies on this cluster.

Finally, we cross-matched the UVIT detected stars with ground-based *V, I* photometry provided by P. Stetson (2017, private communication). In Figure 9, we present the CMD obtained by cross-matching with the ground data, where the UVIT CMD is on the lower-right panel and the corresponding optical CMD is in the left panel. It can be seen that the number of cross-matched stars from the ground data (59 stars) is much less than the number of stars from the *HST* data (254 stars), which cover the inner $0'\!.5$–$3'\!.36$ region. Nevertheless, we detect all three types of HB stars in the ground photometry (28 RHB, 6 HBHB, 13 VBHB), as well as 12 blue straggler stars. By comparing the inner data from the *HST* and the outer data from the ground, it can be seen that most of the HB stars are located within a region of diameter $0'\!.5$–$3'\!.36$. Indeed, only a modest fraction of the detected stars $(47/232 \sim 20\%)$ are found outside this region.

4. Characterizing the HB Population

We have attempted to characterize the HB stars by comparing the UV-optical CMDs with predictions from the stellar evolutionary models. Before proceeding, we note that (Gratton et al. 2012) studied the HB population in NGC 1851 using medium-resolution spectroscopy and found that, on average, the RHB stars have [Fe/H] = −1.14 ± 0.01 dex from Fe I lines and [Fe/H] = −1.20 ± 0.01 dex from Fe II lines. They also measured a He abundance of $Y = 0.291 \pm 0.055$, and estimated an initial He abundance of about $Y = 0.248$, with mild He enhancement thereafter. A large initial He abundance was deemed unlikely.

Figure 8 suggests that the isochrone generally fits the HB well, except for the deviation noticed in the V-BHB stars. The isochrone also suggests fainter extension to the RHB. These deviations could suggest that one or more parameters corresponding to the plotted isochrone might vary among the detected HB stars. We also used the BaSTI models to generate isochrones with different ages and abundances, instead of the Padova models. As we need to fold the UVIT filters into the FSPS models, we are able to change only the age and metallicity of the isochrones, and must keep the other parameters, such as Y_{ini}, constant. In Figure 10, we show isochrones for two ages. In each plot, we have kept the age constant and varied the metallicity as shown in the figure. These isochrones have $Y_{ini} = 0.25$. The figure shows how the isochrones for the HB stars change in the UV with age and metallicity, as per the predictions from BaSTI models. The isochrones shown in both the figures could be used to derive the range of age and metallicity. With the decrease in the value of [Fe/H], the extent of the HB shrinks such that the red end of the HB gets bluer. The presence of an extremely extended HB, as seen in this cluster, can be fitted using isochrones with [Fe/H] ~ -1.0. The fitted value of [Fe/H] is, within the errors, in good agreement with the values obtained by Gratton et al. (2012).

From the upper panel of Figure 10, it is clear that the RHB can be fitted using an isochrone of age 10 Gyr, for the above value of [Fe/H], whereas none of the isochrones in the bottom figure fits the RHB. The bottom figure shows that the fit of the RHB cannot be reproduced by an increase in age. None of the isochrones in the top and bottom panel are able to fit either the V-BHB or the H-BHB. A close examination of the bottom figure suggests that the isochrone shown in green points, corresponding to 12 Gyr, is the closest fit observed for the H-BHB stars. Thus, we find that an age range of up to 2 Gyr might be required to fit the full HB stars, for a constant Y_{ini} and metallicity. In Figure 11, we show the CMD with isochrones of two ages (10, 12 Gyr) for Fe/H ~ -1.0 and $Y_{ini} = 0.25$, for the UV-optical CMDs. These are the parameters we are able to derive for the HB stars using the BASTI isochrones. In summary, we detect the presence of two age groups in the HB of NGC 1851, using the BaSTI isochrones. We find that the RHB stars in the cluster could
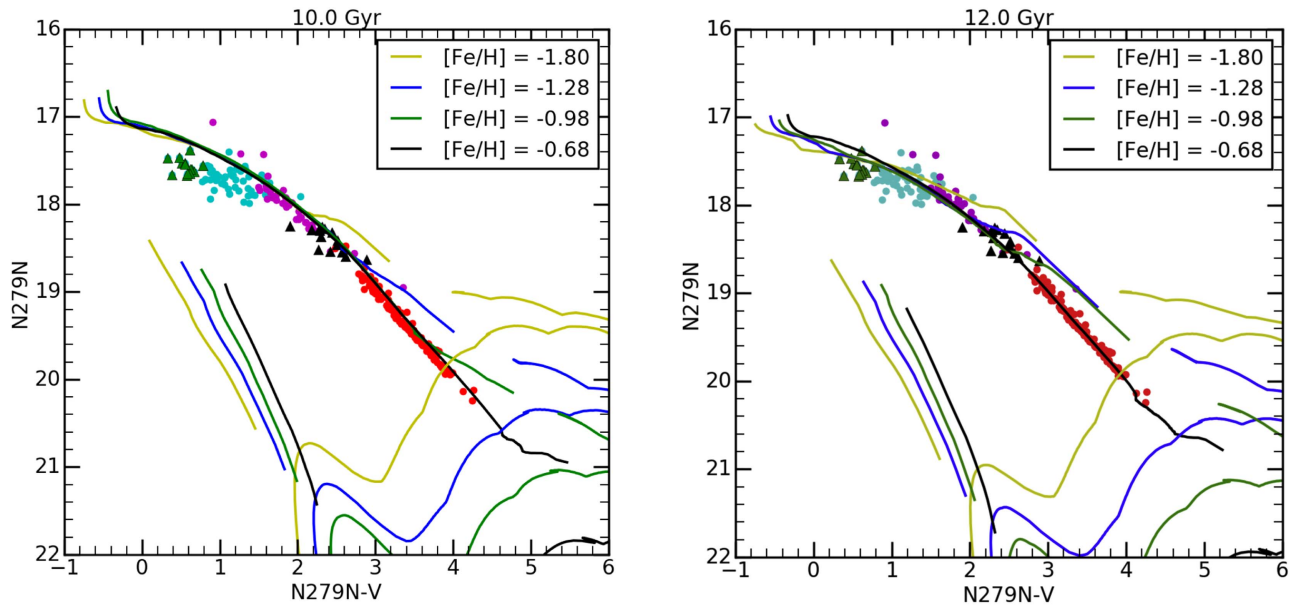
Figure 10. NUV-optical CMD for NGC 1851, based on UVIT imaging in the N279N filter. BaSTI Isochrones are shown for four different values metallicities, as indicated in the legend, and for two assumed ages: 10 and 12.0 Gyr (left and right panels, respectively).
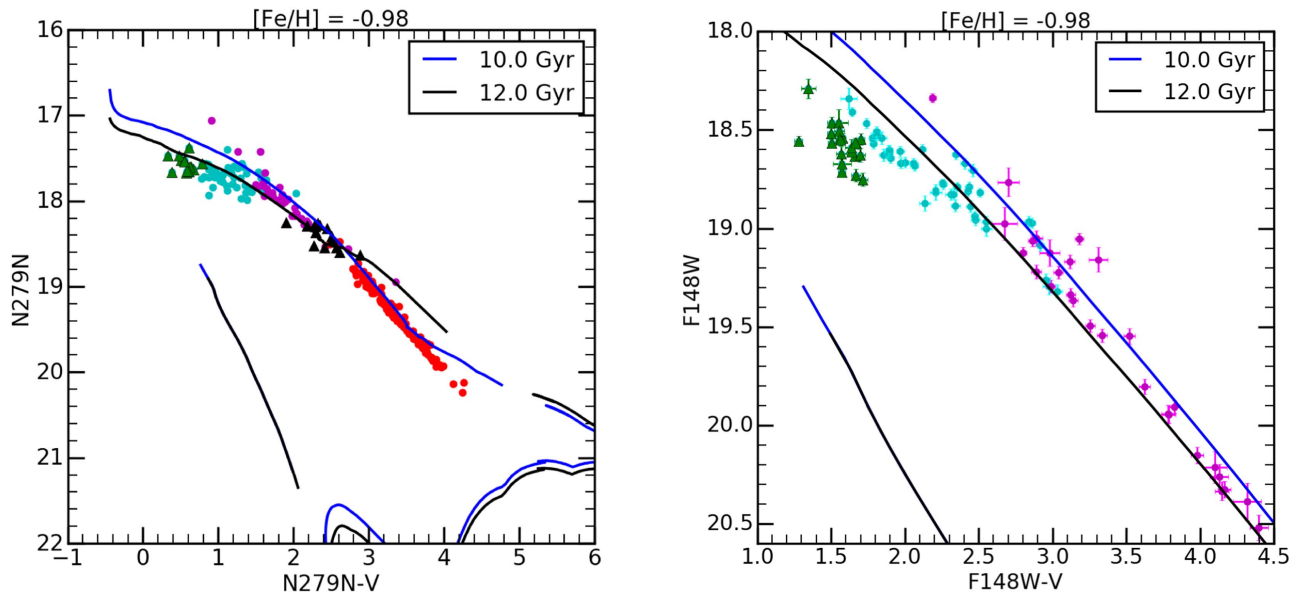
Figure 11. NUV-optical CMD for NGC 1851, based on UVIT imaging in the N279N filter in the upper panel, and FUV-optical CMD for NGC 1851, based on UVIT imaging in the F148W filter in the bottom panel. BaSTI Isochrones are shown for two different ages, as indicated in the legend, and a metallicity of [Fe/H] = −0.98 dex.

belong to a relatively younger population (10 Gyr), whereas the BHB stars could be up to 2 Gyr older. We believe that there cannot be a large difference in [Fe/H] among the HB stars. Recall that Carretta et al. (2011) and Gratton et al. (2012) suggested that the cluster has two populations, with an age difference of up to 2 Gyr.

As noted above, the N279N filter is centered around the Mg II line; therefore, the flux in this filter depends on the Mg abundance of the HB stars. Gratton et al. (2012) found a higher abundance of Mg for their BHB stars, in comparison to the RHB stars. The isochrones in this filter are expected to capture the details of variation in Mg abundance across the HB. The fact that the FUV CMDs also suggest the deviation of V-BHB stars from the 10 Gyr isochrone suggests that the deviation may

not be related to any residual variation in the Mg II strength. This is confirmed from the bottom panel of Figure 11, where we have overlaid the isochrones onto the FUV CMD. The CMD confirms that the V-BHB stars are reasonably well-fitted by the 12 Gyr isochrone. The blue hook stars are fainter than the rest of the V-BHB stars and the isochrones do not reproduce this feature. Thus, we note that the blue hook stars appear to be fainter in the FUV, even though they have normal NUV flux. This may provide some specific clues to their structure and evolutionary phase. Dalessandro et al. (2011) presented the FUV-optical CMD of NGC 2808 and used it to confirm the multi-model distribution of stars along the HB. They found that the canonical models are not able to match the hot end of the HB.

4.1. He Enrichment

The issue of He enrichment in this cluster has been discussed and contested for some time. The spectroscopic study of Gratton et al. (2012) and SGB study of Milone et al. (2008), as well as the HB simulations of Salaris et al. (2008), found no significant enhancements in He. Han et al. (2009) and Kunder et al. (2013), suggested that He is enhanced in the BHB stars, apart from them being older. Joo & Lee (2013) also argued that He enhancement can explain the age effect, and therefore an apparent age difference may actually be due to differences in He content.

In order to understand the effect of Y_{ini} on the HB morphology, we considered the He-enhanced models. The synthetic HB models presented here are based on Y^2 stellar evolutionary tracks with enhanced initial He abundance (Lee et al. 2015). We adopt the Reimers (1977) mass-loss coefficient $\eta = 0.5^{11}$ and the mass dispersion on HB stars $\sigma_M = 0.015\,M_\odot$. We assume a fixed α-element enhancement of $[\alpha/\mathrm{Fe}] = 0.3$. We refer the reader to Chung et al. (2017) for more detailed descriptions of our synthetic HB models. Note that we did not consider the effect of the CNO abundance anomaly in the models. Therefore, the variation of HB morphology is solely coming from the combinations of the metallicity, age, and initial He contents.

In Figure 12, we present the synthetic HB plotted over the observed HB. The left panels show the fit to the observed HB in optical colors of $V - I$. We applied different values of Y_{ini} for the bimodal HB morphology and splits on the sub-giant branch stars of NGC 1851 at the same time. We assume the He-enhanced population consists of a slightly metal-rich population and fix the age of the two population as 12 Gyr. There are still issues in CNO abundance variation between two populations of NGC 1851—however, as reported in Joo & Lee (2013), the variation is less than 0.1 dex, which has almost negligible effects on HB morphology and splits of SGB stars. Therefore, both the HB morphology and the SGB splits are caused by the difference in initial helium abundances. In the right panels, we present the UV CMDs, based on the same stellar parameters as the left panels. The synthetic HB reproduces the RHB and BHB stars very well, though we see that the model predicts fainter BHB stars in the V band and brighter BHB stars in the N279N filter. The difference between the model and the observed magnitude in N279N is more than 3σ. Thus, the synthetic CMD models with He enhancement suggest the following parameter combination for the HB population: an age of 12 Gyr and range in Y_{ini} of 0.23–0.28, with a metallicity range of $[\mathrm{Fe/H}] \sim -1.2$ to -1.3. In particular, the parameter ranges for the RHB stars are $Y_{ini} = 0.23$, 12 Gyr, and $[\mathrm{Fe/H}] = -1.3$, whereas those for the BHB are, $Y_{ini} = 0.28$, 12 Gyr, and $[\mathrm{Fe/H}] = -1.2$. These parameters are estimated from the UV CMDs for the first time and are in good agreement with the previous estimated values of Y_{ini}, $[\mathrm{Fe/H}]$, and age in the literature.

In order to explore population difference among the BHB stars, we used the two FUV filters in the UVIT to produce a F148W versus (F148W−F169M) CMD. Here, the color term

corresponds to the ratio of flux within the FUV band. The F148W is an FUV window with 1300–1800 Å coverage, whereas the F169M filter has 1450–1750 Å coverage. The CMD is shown in Figure 13. We have overlaid the BaSTI isochrones in the upper panel and the synthetic HB from Y^2 models in the lower panel. The photometric errors are also shown for better comparison. The H-BHB stars span a range of 3 mag, whereas the V-BHB stars span a range of one magnitude, with the blue-hook stars co-located with the brightest V-BHB stars. The color difference for the H-BHB stars is ~0.3 mag, whereas it is about ~0.1 mag for the V-BHB stars. The brightest of the H-BHB stars have colors similar to the V-BHB stars. The HB stars tend to be bluer than the predictions, suggesting that they are relatively hotter. On the other hand, we do not see a significant color difference between the H-BHB and V-BHB stars, more than what is suggested by the isochrone. The temperature of the brightest BHB stars, as per BaSTI as well as Padova models, is found to be $\sim12,000$ K. The Y^2 models reproduce the BHB stars better, and the best-fit parameters for the H-BHB stars are 12 Gyr, $Y_{ini} = 0.28$, and $[\mathrm{Fe/H}] \sim -1.2$ dex. They also predict the BHB stars to be more then 1 mag brighter than the observed BHB stars in the F148W filter. This needs further attention. The estimated parameters are in overall agreement with Gratton et al. (2012).

5. Spatial Distribution of HB Stars

Milone et al. (2008) divided stars on the sub-giant branch into faint (fSGB) and bright (bSGB) populations, with 45% and 55% of the stars belonging to these two components. They found the HB to be bimodal as well, with $63\% \pm 7\%$ and $37\% \pm 9\%$ associated with the red and blue branches, respectively. In our data, cross-matched against the *HST* data, we detect 232 HB stars in total, with 131 stars ($\sim56\%$) on the RHB and and 101 stars ($\sim44\%$) on the BHB. These fractions are similar to those found by Milone et al. (2008) for SGB and HB stars. The spatial distribution of the SGB and HB components were found to be the same by Milone et al. (2008). The radial distribution of HB stars detected by UVIT and cross-matched to *HST* are shown in Figure 14. The upper panel shows the distribution of V-BHB, H-BHB, and RHB, with the same color code as in the earlier figures. In the bottom panel, we have combined the V-BHB and H-BHB stars into a single group (BHB) and their radial distribution (blue line) is shown along with the distribution of RHB stars (red line). We note that the inner regions ($\leqslant1'$) have more BHB stars. Beyond $\geqslant1'.4$, we see an excess of RHB stars, as suggested by the crossover of the two distributions. A K–S test for this pair of distributions (bottom panel) returns a probability of 2%, which suggests that the two populations differ in their radial distribution. The data used here for K–S test are those detected by UVIT from the original *HST* sample. Due to crowding, we were not able to detect stars in the central $\sim10''$, highlighting that our data suffers from incompleteness in the core. Milone et al. (2008) found that the probability that the BHB and RHB stars are drawn from the same sample is 19%. Therefore, radially, the BHB and the RHB distributions may only be marginally different.

In Figure 15, we show the spatial distribution of the BHB stars in the upper panel and the histogram of the azimuthal distribution in the lower panel. We converted the HB stars to an *XY* coordinate system with origin at the cluster center. In the

---

[11] In order to reproduce the HB morphology of inner halo MWGCs, we assume the age of the inner halo to be 13.3 Gyr and the initial helium $Y_{ini} = 0.23$. Because the increased eta value has the same effect as increased age or increased initial helium abundance (decreasing the mean mass of HB stars), if we increase the initial helium or include helium spread in the inner halo, the eta becomes less than 0.5.
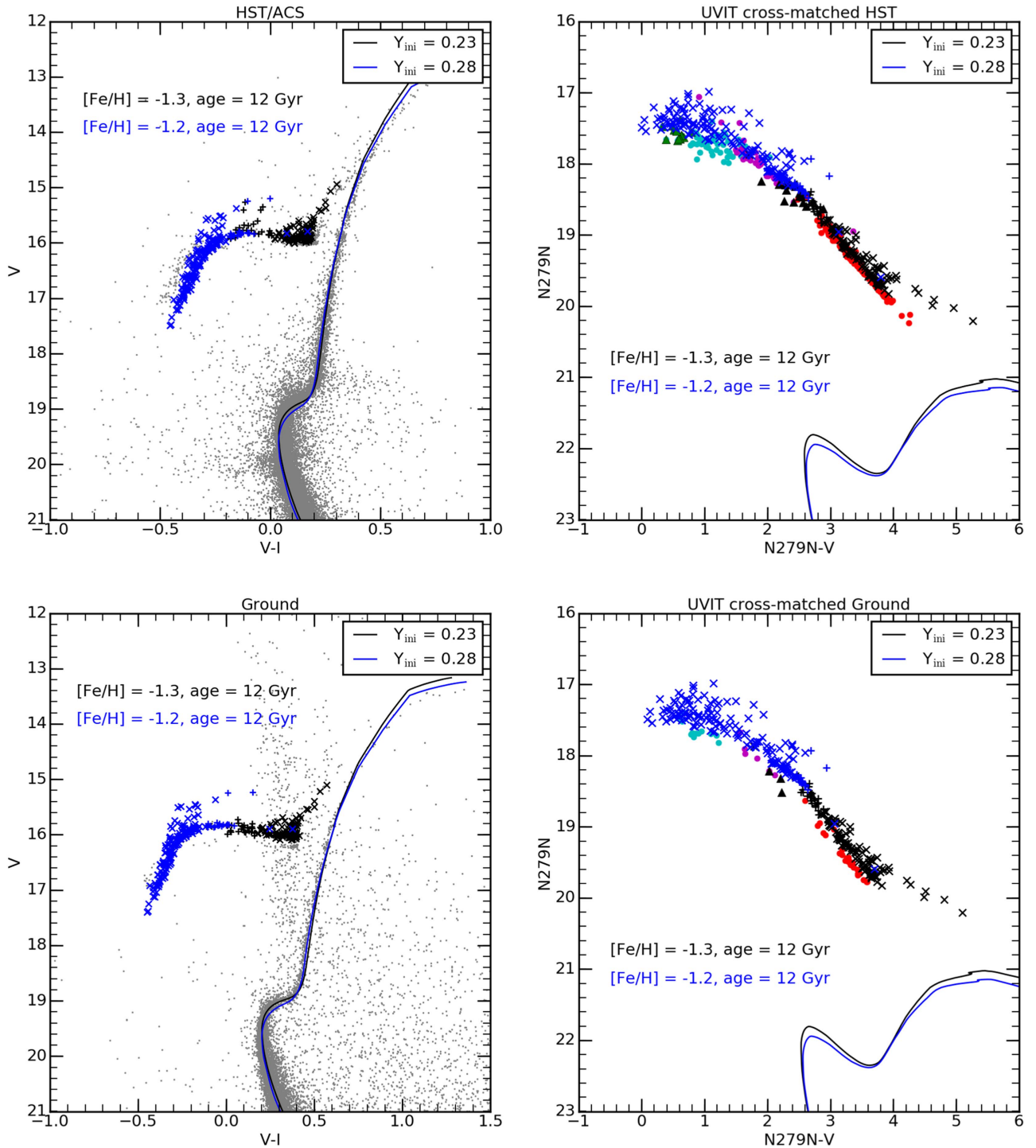
Figure 12. Synthetic HB models from Y^2 stellar evolutionary tracks with enhanced initial He abundance Y_{ini} (Lee et al. 2015) are overlaid on the observed data points. The upper panel shows the *HST* optical data in the left panel, and cross-matched UVIT data in the right panel. The lower panel shows the ground-based optical data in the left panel and cross-matched UVIT data in the right panel. The crosses denote the generated synthetic HB. The lines indicate the Y^2 for the Mg turn-off and SGB.

upper panel, we have color-coded the stars according to their azimuthal angle, ϕ, which increases toward the positive Y axis, starting from the negative X axis. The inner region with data incompleteness ($\sim$10″ radius) is indicated. We have also indicated the half-light radius of the cluster as the dotted circle, with a radius of $r_h = 30\rlap{.}{''}6$ (Watkins et al. 2015). The figure suggests that the BHB stars show a non-uniform azimuthal distribution. In the lower panel, the histogram is shown to bring out the details, where we show a bin width of 30° in azimuth

angle. We also show the average number as a straight line, and the hatched area denotes the 1σ width. We see that two bins are below and one is above this width. Therefore, there are fewer stars in the 60°–90° and 150°–180° bins, whereas there are more stars in the 180°–210° bin.

In Figure 16, we present a similar test for the RHB stars. This also points to an azimuthally non-uniform distribution, albeit one that differs from the BHB stars. The spatial plot suggests that the RHB stars outside the half-light radius are
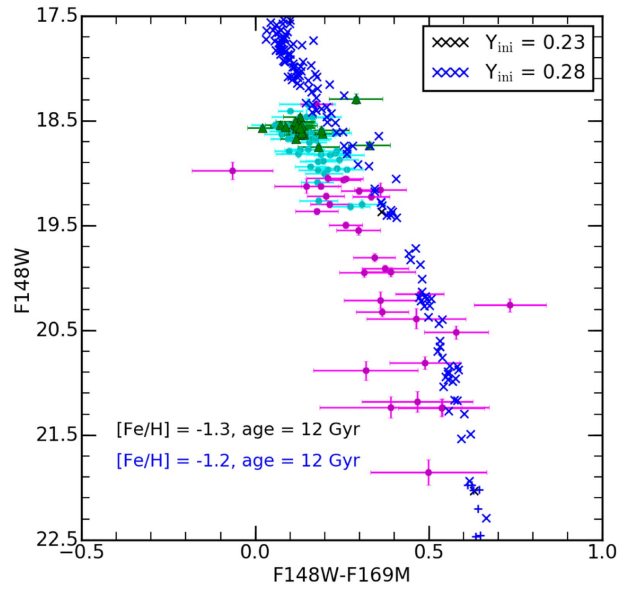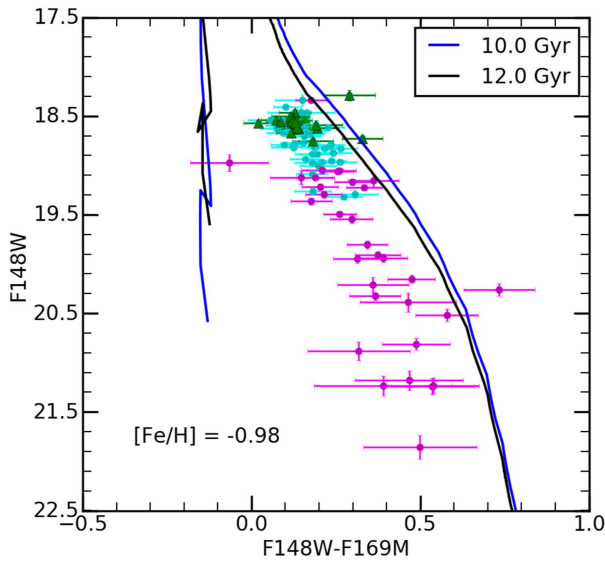
Figure 13. FUV CMD, based on UVIT photometry, for the F148W and F169M filters. BaSTI isochrones at three different ages are shown in the top panel. The synthetic HB from the Y^2 models are shown in the bottom panel.
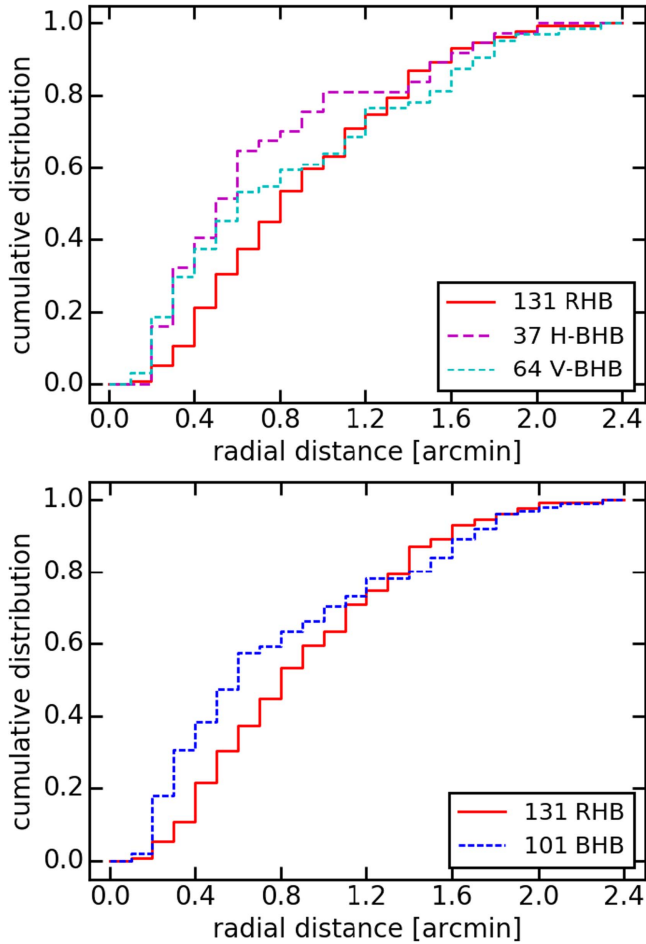
Figure 14. The radial distribution of HB stars. The upper panel shows the distribution of V-BHB, H-BHB, and RHB stars. In the lower panel, the V-BHB and H-BHB stars are combined into a BHB sample and shown along with their RHB counterparts.

preferentially located in three specific values of ϕ. This is indicated by the histogram, which shows a wavy pattern with three peaks and two troughs. Inside the half-light radius, the

RHB stars are located mostly in the first and fourth quadrants, which is different from the distribution seen outside. The histogram shown suggests that two bins (120–150 and 240–270) have fewer stars, whereas the 150–180 bin has more stars than 1σ width. Thus, the RHB stars are also found to show a non-uniform azimuthal distribution. Both the BHB and RHB stars are azimuthally asymmetric, suggesting that they may not be mixed well. The spatial distribution presented by Milone et al. (2008) shows similar features (i.e., see their Figure 7). The analysis provided here uses all stars outside the central 10″. The missing inner stars could alter the radial distribution, but may not affect the azimuthal distribution. As the number involved is not large, we do not attempt to derive the statistical significance of the azimuthal variation. Our finding could provide additional support for the possibility that this cluster is a merger remnant (Carretta et al. 2011).

6. UV Variability of RR Lyrae Stars

Oosterhoff (1939) showed that Galactic GCs, according to their RR_{ab} Lyrae stars, are divided into two distinct groups—one with RR_{ab} periods of 0.55 day (Oosterhoff type I or OoI) and the other with periods of 0.65 day (Oosterhoff type II or Oo II) for RR_{ab} stars. Oo I clusters have around 75% of their RR Lyrae pulsating in the fundamental mode, whereas it is about 50% for Oo II types. Oo I clusters tend to be more metal-rich and host fainter RR Lyrae variables than OoII clusters (Caputo et al. 2000).

In the specific case of NGC 1851, Walker (1998) identified 29 RR Lyrae variables in the cluster and found the ratio of first-overtone RR Lyrae to fundamental-mode RR Lyrae stars to be consistent with Oo II clusters (although near the end of Oo I distribution). This cluster is known have the most extreme (long) period for RR_{ab} stars; this is considered to be an unusual OoI object (Downes et al. 2004; Kunder et al. 2013). It has been difficult to conclude whether the differences in the intrinsic magnitudes of RR Lyrae variables in Oo I and Oo II clusters are caused by something other than just metallicity, such as age or helium content. In this cluster, where an internal spread in [Fe/H] is modest, at best, Kunder et al. (2013)
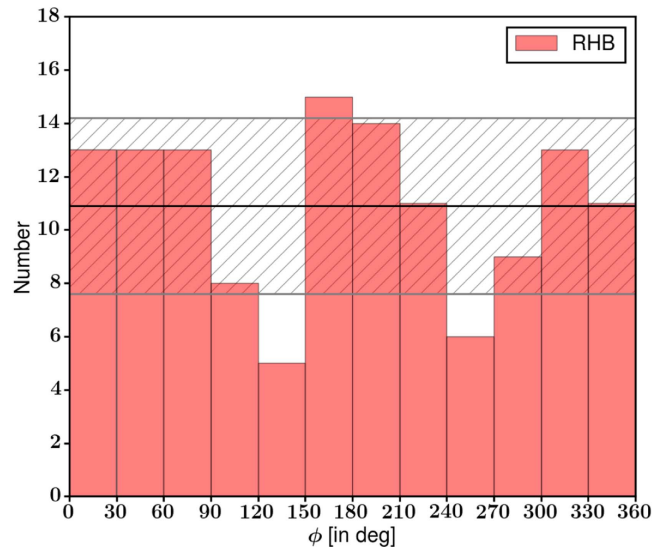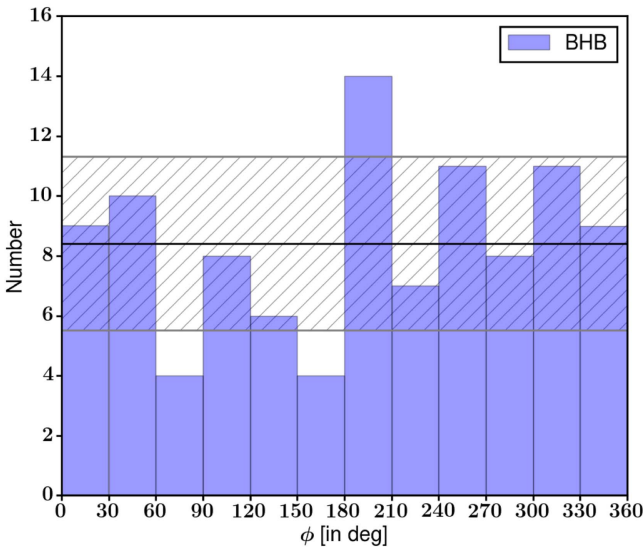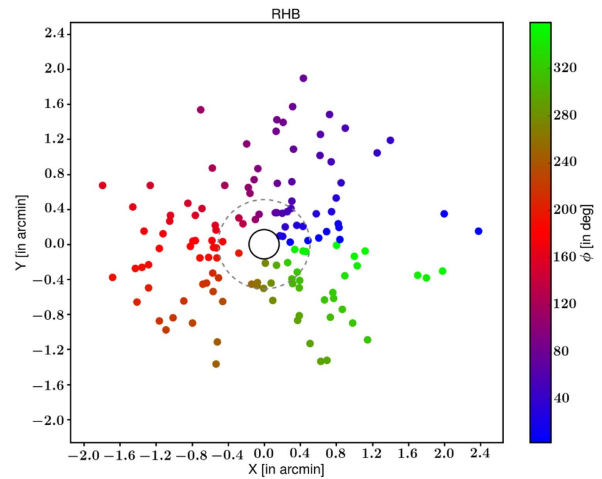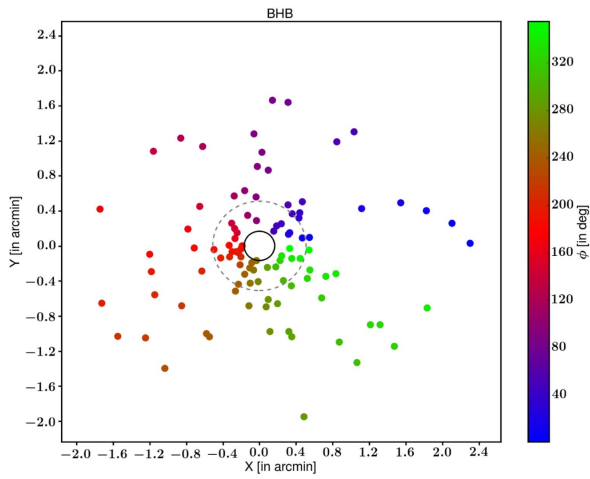
Figure 15. The spatial distribution of BHB stars in NGC 1851. On the left, we plot the distribution of BHB star in the cluster. The origin marks the cluster center, while the inner circle (10″) corresponds to the region with significant sample incompleteness, and the outer circle corresponds to the half-light radius (30.″6, Watkins et al. 2015). The panel on the right shows the histogram of position angles, using a bin width of 30°. The straight line shows the mean value and the hatched region shows the 1σ error width.

Figure 16. Same as Figure 14, except showing the distribution of RHB stars within the cluster.

suggested that a difference in He abundance among the RR Lyrae variables could explain the observed periods, amplitudes, and brightnesses. In the optical, RR Lyrae stars have typical amplitudes of 0.5–1.0 mag, whereas our UV data show much larger variations. For instance, (Downes et al. 2004) identified 11 RR Lyrae-like variables in the core of the cluster using the *HST* FUV data. They found the amplitudes of these stars to be as large as 4 mag. Their Figure 3 shows the light curves of RR Lyrae stars in the FUV (although these are not complete light curves).

Our UVIT observations of NGC 1851 were taken over multiple orbits, as a consequence of the early operations of Astrosat. Variable stars were thus sampled over a range of their cycles that would not have been possible in a single pointing. We used the RR Lyrae stars from Walker (1998) and Kunder et al. (2013) to cross-match our sample. The RR Lyrae stars that we have detected are shown in Figures 17 and 18. In all, we find 12 known and two new variables (red and green

squares, respectively) in the FUV. In the NUV, we find 18 previously known and three new variable stars. This brings the total of RR Lyrae-like variables in this cluster to 43: i.e., 29 RR Lyrae stars were known from Walker (1998) and another 11 from Downes et al. (2004). In the upper panel of Figure 19, we present full light curves of two RR Lyrae stars in the FUV and NUV filters. These light curves demonstrate the structure of the variability in the FUV and the NUV. It can be seen that, in the FUV, the RR Lyrae stars are almost non-detectable except during the maximum light, whereas there is a measurable flux through the whole cycle in the NUV. We can also notice a larger amplitude in the FUV than in the NUV. In order to bring out these features of the light curves, we created a "typical" light curve profile. A "typical" light curve is the mean of several individual ones created by a) cross-correlating the phased plots to match the maxima, and b) taking the mean of the NUV and FUV phase-shifted values in bins of 0.05 phase. This is presented in the lower panel of Figure 19. The characteristic of the UV light curves is that the maxima are much sharper and the slow decline seen in visible wavelengths almost disappears.
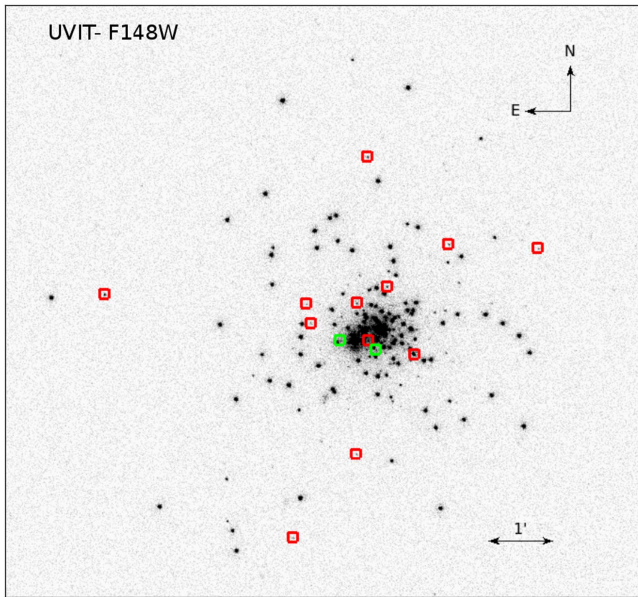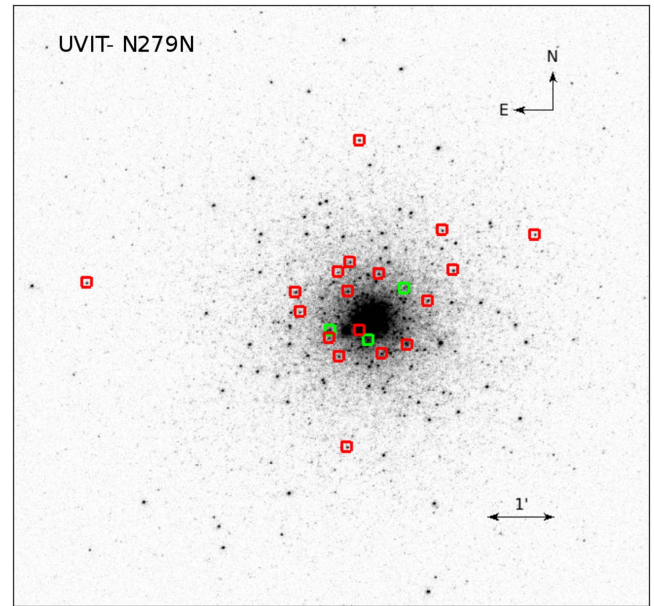
Figure 17. RR Lyrae stars in NGC 1851, identified from our the FUV UVIT images. Two newly detected variables are shown in green. North is up and east is to the left in this image, which measures $1'$ on a side.

Figure 18. RR Lyrae stars in NGC 1851, identified from our the NUV UVIT images. Three newly detected variables are shown in green. North is up and east is to the left in this image, which measures $1'$ on a side.

Our analysis of the HB population suggests that there could be RR Lyrae stars belonging to the RHB as well as the BHB stars. As noted above, our results suggest that there is an age and/or He difference between the BHB and the RHB. Our model HB population shows the presence of two Y_{ini} population in the region of the RR Lyrae stars. Therefore, our analysis supports a difference in age or/and Y_{ini} as the possible reason for the RR Lyrae properties in the cluster, and perhaps the Oosterhoff dichotomy.

7. Discussion

In this study, we have presented FUV and NUV CMDs obtained from the UVIT on *ASTROSAT*. The superior image quality of the UVIT, along with the filter systems in the FUV and NUV channels have made this work possible. The UVIT images shown in the Figures 1, 2, and 3 demonstrate that the UVIT is capable of producing excellent UV images of Galactic GCs. The calibration of the UVIT filter systems is complete (Tandon et al. 2017), and the effective areas as well as the zero-points are used to create the CMDs and isochrones in the UVIT filters. We have also demonstrated that simultaneous observations in FUV and NUV help in detecting variable stars. Our study has also added three RR Lyrae-like stars to the previous catalog of 40 variables.

As it is difficult to identify evolutionary sequences in the UV CMDs, we used the *HST*-ACS data to cross-match and identify them. We detect mostly HB stars and a few blue straggler stars. We divided the detected HB into RHB, V-BHB, and H-BHB stars. We also detect a few blue hook stars in this cluster, appearing at the end of the vertical extension of the HB; their temperature is estimated to be ~12,000 K. This study demonstrates the ability of UV studies to bring out the details of HB population in GCs. We have analyzed the UV CMDs with the help of isochrones generated in the UVIT filters, using the FSPS code (Conroy et al. 2009). We compared the CMDs with Padova as well as BaSTI isochrones, and the synthetic HB using the Helium enhanced Y^2 models.

NGC 1851 is one of the many GCs now known to host multiple stellar populations. Evidence in this particular cluster comes primarily from the detection of two SGB sequences in the *HST* data (Milone et al. 2008; Piotto et al. 2012). Spectroscopic studies performed on RGB (Carretta et al. 2011) and HB stars (Gratton et al. 2012) support the existence of multiple populations. We used a distance modulus of 15.52 mag (Cassisi et al. 2008). As the reddening is minimal toward this cluster (Harris 1996), we have not incorporated reddening correction. The fit between the observed data and the models do have a slight dependency on these parameters. We identify and locate the full stretch of the HB stars in the UV CMDs, within the inner $4'.0$ diameter of the cluster. BaSTI models suggest that the HB populations in NGC 1851 may have an age difference of ~2 Gyr, for a constant metallicity of [Fe/H] ~ −1.0 dex and Y_{ini} ~ 0.25. We are able to characterize two HB populations using the Y^2 models and the generated synthetic HB. The best fits were obtained for an age range of ~12 Gyr, with a more or less similar [Fe/H] of ~−1.3−1.2, and for two values of Y_{ini}, ~0.23 and 0.28. The takeaway point is that neither model supports the presence of super-He-rich stars in the HB. There could be a moderate age difference (~up to 2 Gyr) or a moderate helium enrichment (~up to 0.05 dex) among the HB stars. This is the first time the HB parameters have been estimated from UV observations for this cluster. These are in agreement with those estimated from optical studies. Our observations are not deep enough to detect the sub-giant branch, which could have added more constraints on the estimated parameters. We plan to carry out deeper observations of more GCs, as part of a broader program to carry our UVIT imaging of Galactic GCs.

The RHB and BHB stars, which were found to have a marginal difference in their radial distribution, were also found to have a non-uniform azimuthal distribution outside the cluster's central $10''$. The uncorrelated and individually non-uniform distribution of the BHB and RHB stars suggest that these two populations are not mixed very well. This could provide support for the hypothesis that this cluster is a merger

13
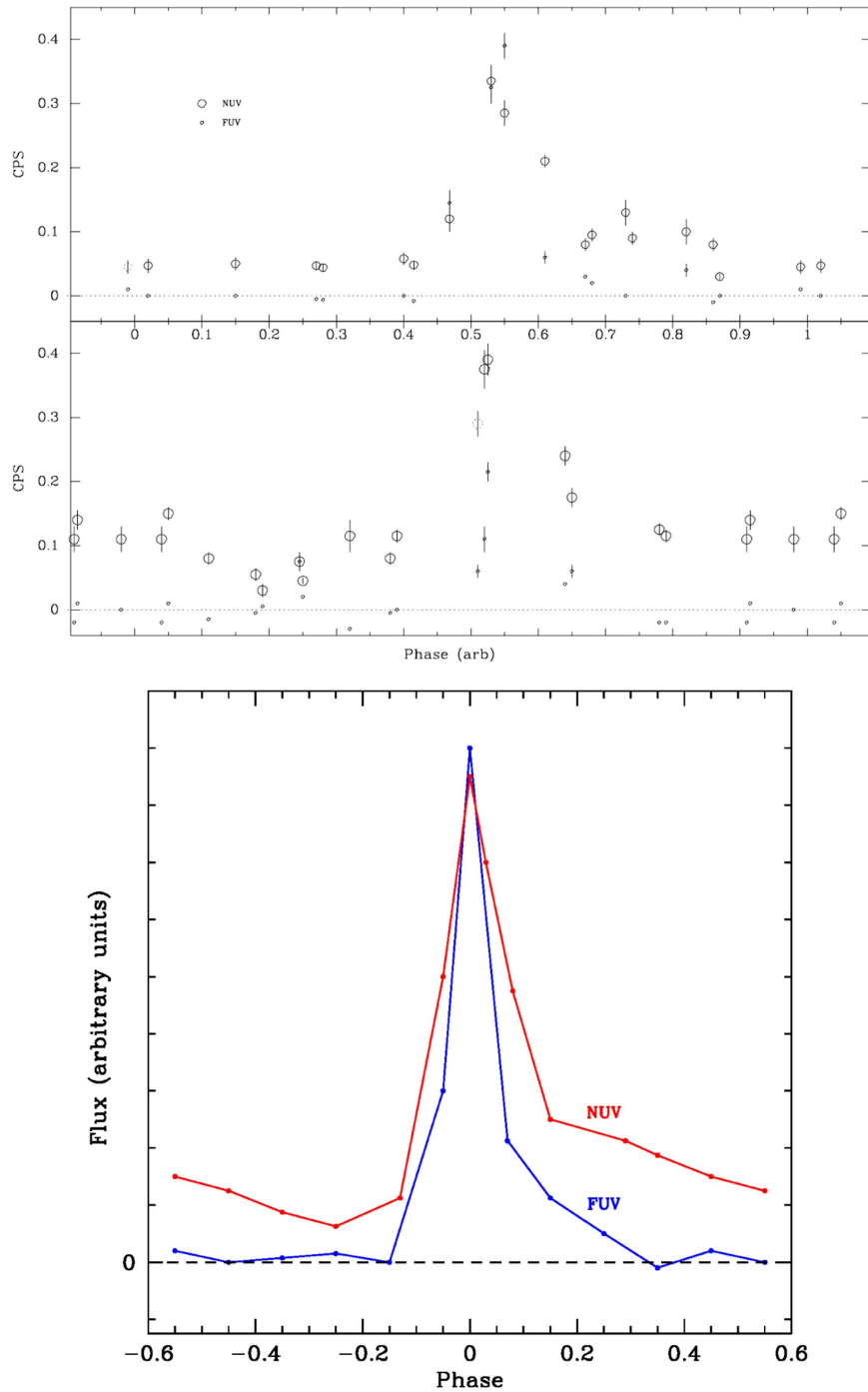
Figure 19. Upper panel shows the full light curves of two RR Lyrae stars in NGC 1851. These full light curves and the rest of the partial light curves were used to create a typical light curve for the FUV and NUV, as shown in the lower panel.

remnant. We note that, if the merger is recent, the populations still may not be well mixed. The merging between the two progenitor clusters could have occurred recently, as the relaxation time at the half-mass radius is about 0.3 Gyr (Harris 1996), whereas the full cluster relaxation takes about 2–3 relaxation times (Carretta et al. 2011).

Because UVIT is operated in photon-counting mode, we are able to detect variability of known RR Lyrae stars in both the FUV and NUV bands. We also are able to create typical light curve in FUV and NUV wavelengths. These observations confirm the large amplitude variations of RR Lyrae stars previously seen in UV passbands, when compared to the optical.

We find that the detected RR Lyrae stars may be belong to the RHB or the BHB. As mentioned earlier, RR Lyrae stars in this cluster are known to belong to Oo I, with properties similar to Oo II. As we find age and helium abundance to be the main difference among the HB stars in this cluster, it is likely that the differences among the RR Lyrae stars and the Oosterhoff classification may be due to these two parameters.

8. Conclusions

The first GC images from the UVIT on the Indian multi-wavelength astronomy observatory, *ASTROSAT*, are presented

here. The superior image quality of the telescope helps to almost resolve the core of the GC NGC 1851. The large field of view of the UVIT helps to detect UV stars beyond the central region of the cluster. PSF photometry of ∼300 stars in two FUV filters and ∼2300 stars in one NUV filter is used to make UV CMDs. We are able to compare and match the *HST*-detected stars in the center of this cluster. Thus, we prove that the UVIT images in the FUV, in combination with the *HST* data, are a very powerful tool to understand the stellar population in the core of GCs. We also generated isochrones in the UVIT filter system that are used to compare the observed CMDs, particularly the HB distribution. We have detected the full HB extent, including blue hook stars and RR Lyrae stars. We have identified three new RR Lyrae-like variables in the cluster, which raises the number of RR Lyrae-like stars to 43. The simultaneous observation of the FUV and NUV channels in photon-counting mode helped in the identification of RR Lyrae stars in the FUV and the NUV bands. We used the Padova and BaSTI isochrones to compare the observed HB. The BaSTI models suggest two populations among the HB stars, which are likely to have similar metallicity ([Fe/H] ∼ −1.0) and He abundance, but with two different ages (10 and 12 Gyr). The Y^2 models and the generated synthetic HB suggest one population with an age of 12 Gyr, $Y_{ini} = 0.23$, and [Fe/H] ∼ −1.3, and another population of same age (12 Gyr) and similar Fe/H] ∼−1.2, but with enhanced $Y_{ini} = 0.28$. The distribution of BHB and the RHB stars were found to suggest that the populations are not well-mixed, which could lend support to the idea that NGC 1851 is probably a recent merger remnant.

ORCID iDs

Patrick Côté ⊙ https://orcid.org/0000-0003-1184-8114
S. K. Ghosh ⊙ https://orcid.org/0000-0003-0329-2160
J. Murthy ⊙ https://orcid.org/0000-0003-4034-5137

References

Caputo, F., Castellani, V., Marconi, M., & Ripepi, V. 2000, MNRAS, 316, 819
Carretta, E., Lucatello, S., Gratton, R. G., Bragaglia, A., & D'Orazi, V. 2011, A&A, 533, A69
Cassisi, S., Salaris, M., Pietrinferni, A., et al. 2008, ApJL, 672, L115
Chung, C., Yoon, S.-J., & Lee, Y.-W. 2017, arXiv:1704.07382
Conroy, C., Gunn, J. E., & White, M. 2009, ApJ, 699, 486
Dalessandro, E., Salaris, M., Ferraro, F. R., et al. 2011, MNRAS, 410, 694
Downes, R. A., Margon, B., Homer, L., & Anderson, S. F. 2004, AJ, 128, 2288
Gratton, R. G., Lucatello, S., Carretta, E., et al. 2012, A&A, 539, A19
Han, S.-I., Lee, Y.-W., Joo, S.-J., et al. 2009, ApJL, 707, L190
Harris, W. E. 1996, AJ, 112, 1487
Joo, S.-J., & Lee, Y.-W. 2013, ApJ, 762, 36
Kunder, A., Salaris, M., Cassisi, S., et al. 2013, AJ, 145, 25
Lee, Y.-W., Joo, S.-J., Han, S.-I., et al. 2015, HiA, 16, 247
Marigo, P., & Girardi, L. 2007, A&A, 469, 239
Marigo, P., Girardi, L., Bressan, A., et al. 2008, A&A, 482, 883
Milone, A. P., Bedin, L. R., Piotto, G., et al. 2008, ApJ, 673, 241
Olszewski, E. W., Saha, A., Knezek, P., et al. 2009, AJ, 138, 1570
Oosterhoff, P. T. 1939, Obs, 62, 104
Pietrinferni, A., Cassisi, S., Salaris, M., & Castelli, F. 2004, ApJ, 612, 168
Piotto, G. 2009, in IAU Symp. 258, The Ages of Stars, ed. E. E. Mamajek, D. R. Soderblom, & R. F. G. Wyse (Cambridge: Cambridge Univ. Press), 233
Piotto, G., Milone, A. P., Anderson, J., et al. 2012, ApJ, 760, 39
Piotto, G., Milone, A. P., Bedin, L. R., et al. 2015, AJ, 149, 91
Postma, J. E., & Leahy, D. 2017, PASP, 129, 115002
Reimers, D. 1977, A&A, 57, 395
Salaris, M., Cassisi, S., & Pietrinferni, A. 2008, ApJL, 678, L25
Sarajedini, A., Bedin, L. R., Chaboyer, B., et al. 2007, AJ, 133, 1658
Schiavon, R. P., Dalessandro, E., Sohn, S. T., et al. 2012, AJ, 143, 121
Subramaniam, A., Tandon, S. N., Hutchings, J., et al. 2016, Proc. SPIE, 9905, 99051F
Tandon, S. N., Hutchings, J. B., Ghosh, S. K., et al. 2017, JApA, 38, 28
Tandon, S. N., Subramaniam, A., Girish, V., et al. 2017, AJ, 154, 128
Walker, A. R. 1992, PASP, 104, 1063
Walker, A. R. 1998, AJ, 116, 220
Watkins, L. L., van der Marel, R. P., Bellini, A., & Anderson, J. 2015, ApJ, 803, 29
Yong, D., & Grundahl, F. 2008, ApJL, 672, L29